SUPPLEMENTARY INFORMATION

Near-surface Wetland Sediments as a Source of Arsenic Release to Ground Water in Asia

Matthew L. Polizzotto, Benjamin D. Kocar, Shawn G. Benner, Michael Sampson, and Scott Fendorf

Supplementary Information

Summary
This supplement provides additional methods, field area description, groundwater flow calculations, numerical modeling results, dissolved and solid-phase chemical data, and mass balance calculations from our study of the Upper Mekong Delta, Cambodia. The material is organized as 7 sections with an appendix and includes 4 tables and 9 figures.

Outline
Additional methods are described in Section 1 of the Supplementary Information. Section 2 provides information about the geologic history, stratigraphy (Supplementary Figure 1), aqueous chemistry (Supplementary Table 1), and land use practices within our field area. Groundwater flux calculations are presented in Section 3, including hydraulic heads throughout the field area (Supplementary Figures 2 and 3), hydraulic conductivity results (Supplementary Tables 2), and flow distances (Supplementary Table 2). The results of groundwater flow modeling (Supplementary Table 4 and Supplementary Figures 4 and 5) are shown in Section 4. Section 5 discusses the spatial distribution (Supplementary Figures 6 and 7) and temporal variations (Supplementary Figure 8) of dissolved arsenic concentrations and solid-phase redox profiles of arsenic (Supplementary Figure 9). Section 6 outlines arsenic input and output calculations. Supplementary Information references are given in Section 7, and all groundwater arsenic measurements are presented in the Supplementary Information Appendix.

Sections

1. Additional Materials and Methods

Analytical measurements. Dissolved Al, Ca, K, Fe, Mg, Mn, Na, P, S, and Si were measured by ICP-AES, and quality control standards were monitored throughout the course of the analyses. Anions (F^-, Cl^-, NO_3^-, PO_4^{3-}, and SO_4^{2-}) were analyzed by standard ion chromatography methods. Dissolved organic carbon (DOC) was measured as non-purgeable organic carbon on a Shimadzu TOC-5000A analyzer (Shimadzu Corporation, Japan). Nitrate and ammonium were analyzed colorimetrically with an Alpkem Continuous-Flow Analyzer (OI Corporation, Texas, USA).

Elemental solid-phase concentrations were determined after microwave digestion according to EPA method 3052[30]. Sediment samples were chemically dissolved in 3:1 concentrated HNO_3:concentrated HF and the resulting solution was evaporated to dryness. Following reconstitution in HCl, concentrations were measured by ICP-AES.

Arsenic distribution. Simple Kriging, a spatial least square estimator, was use to generate the map of As concentrations within a transect spanning the wetland environment to the Mekong river (Figure 3, main text). The model of spatial correlation was illustrated through a variogram with strong anisotropy. All raw data points match values generated from the Kriging.

Hydraulic conductivity determination. Particle size separation was performed on 14 aquifer sand samples and the resulting grain size distributions were used to calculate hydraulic conductivity values. The Breyer method[31] was used to calculate hydraulic conductivities of the fine sand aquifer sediments. For medium and coarse aquifer sand samples, the Hazen method[31] was used to obtain K values.

Constant head permeameter tests[32] were performed on 10 samples from the upper clay layer, with depths ranging from 6 m to 18 m, in order to calculate hydraulic conductivity values. Samples were dried and repacked into sealed flow cells, with lengths of 3.3 cm and cross-sectional areas of 24 cm^2. Constant flow was maintained and monitored. For each sample, the test was repeated with 3 to 6 different heads of pressure; for each trial at all depths at each site, the range of calculated K values was within a factor of 2.

Slug displacement tests were performed on 15 shallow (8-12 m) wells throughout the field area and the resulting head changes were analyzed according to the Hvorslev method[33]. The resulting K values for the falling head and rising head tests were within a factor of 2 from each other in all but one case.

Arsenic solid-phase X-ray fluorescence and X-ray absorption spectroscopy. Spatial distributions of As were determined using X-ray fluorescence (XRF) spectroscopy, and X-ray absorption spectroscopy (XAS) was used to elucidate oxidation and chemical states of arsenic. Experiments were conducted on undulator beamline 13-ID-C at the Advanced Photon Source, Argonne National Laboratory. The ring operated at 7 GeV and current was maintained at ~100 mA through periodic electron injection. Energy selection was performed by a Si (111) monochromator. All sample preparation was conducted

under anaerobic conditions (N_2:H_2, 95:5) in a polyethylene glovebag. Sediments were spread on polycarbonate slides and sealed with Kapton tape. Slides were rastered in 5 μm steps around a 5x6 μm X-ray beam and fluorescent X-rays were measured with a 16-element solid-state energy-dispersive Ge detector. Incident and transmitted intensities were measured with in-line ionization chambers. Multiple X-ray fluorescence maps were made on sediments from each depth. Areas of arsenic concentration in the elemental maps were analyzed with micro-X-ray absorption near-edge structure (μ-XANES) spectroscopy to determine arsenic speciation. The sample spectra were collected from –50 to +100 eV about the As K_α edge of 11867 eV, and speciation was determined through a spectral analysis of first-derivative peaks from the XANES spectra. A dilute sodium arsenate standard was used for energy calibration (11874 eV).

2. Field area

The Mekong River is a broad river that carries the seventh largest sediment load in the world, the majority of which is discharged during the wet season. The delta floodplain is roughly 62,500 km^2 [34] and the upper 10-35 m of sediment has been deposited as a prograding deltaic sequence in the past 6000 y[35] following the most recent sea level high stand.

Our field area in the Kandal province of Cambodia comprises approximately 50 km^2 between the Mekong and Bassac Rivers and is typical of the Mekong floodplain system, with elevated levees along river banks receding to a native, seasonally-flooded wetland basin between the two rivers. The Holocene-age stratigraphy is characterized by a thick grey aquifer sand (with interbedded clay) unit overlain by a 5-22 m clay-silt aquitard unit that extends across the water table (Supplementary Figure 1). This clay-silt unit is characterized by organic rich units that grade from grey-red above the water table to grey-black at depth. Near the base of the sand unit at some locations (particularly proximal to the Mekong and Bassac Rivers), coarse grained sands and gravels are observed. At limited locations within the field site, Holocene sediments are underlain by orange colored Quaternary sands associated with delta aggradation[35].

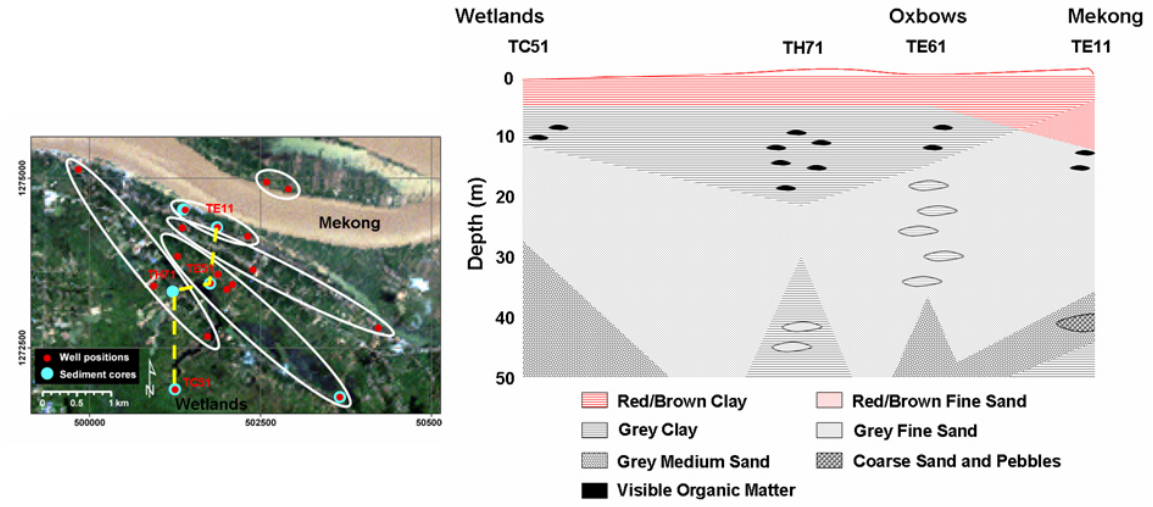

Supplementary Figure 1. Cross-sectional sedimentary diagram of detailed field area. The cross-section in the right panel is taken along the yellow dotted line in the left panel map view. In the map view, blue circles represent locations where intact cores were collected; these samples agreed with samples collected from well drilling cuttings which indicate the dominant clay and sand layers. Drill cuttings were collected and cataloged at each well. White ovals in the map view panel group wells with similar sedimentary profiles.

While drilling and coring techniques did not permit collection of continuous, undisturbed cores, our observed stratigraphy is consistent with the sedimentary profile and history of the upper Mekong Delta proposed by Tamura et al[36]. Carbon dating of the fine-grained sequence indicates that the entire unit was deposited over the previous 7500 years; the

upper, orange colored sediments were likely deposited over the last 700 years[36]. Below the upper clay/silt unit, a distinct transition to sand-rich sediments is observed.

A network of 80 installed wells and 10 surface water monitoring sites are distributed throughout the field area, and a ~5 km^2 focused study area includes near-surface lysimeters and a subset of closely spaced wells for more detailed spatial analyses.

The massive deltas of Asia, inclusive of the Mekong and Ganges-Brahmaputra systems, that drain the Himalayan uplift have formed following the rise in sea level 6,000 to 10,000 years ago. Each system has characteristic inverted and subdued deltaic topography, and associated hydrology is strongly influenced by the monsoonal-driven rise and fall of its respective rivers, with groundwater gradients dominated by the seasonal rise and fall in river levels. Moreover, similar geologic history of the Mekong and Ganges-Brahmaputra has produced similar stratigraphy, most notably a grey sand aquifer overlain by a confining clay unit. Additionally, each system contains diffuse, near crustal-average solid-phase arsenic concentrations.

Groundwater chemistry at our field site is also similar to that in other arsenic-contaminated aquifers throughout Southeast Asia. Dissolved arsenic concentrations are associated with reducing and circumneutral pH conditions (Supplementary Table 1), with an average Eh of 70 mV (relative to the standard hydrogen electrode), pH of 7.1, dissolved O_2 <1 mg L^{-1}, Fe^{2+} of 8.0 mg L^{-1}, SO_4^{2-} of 8.2 mg L^{-1}, and often detectable (>1 μg L^{-1}) HS^-. Groundwaters have high alkalinities such that HCO_3^- provides >70% of the bulk anionic charge in all but 5 of the wells, while Ca^{2+} is the dominant cation and contributes an average of 46% of the bulk cationic charge. Ammonium concentrations average 20 mg L^{-1} and correlate with dissolved organic carbon which averages 6.9 mg L^{-1}.

However, unlike in the Ganges-Brahmaputra Delta, the conditions at our field area provide an opportunity to investigate arsenic behavior in an aquifer subjected to limited anthropogenic disturbance. In appreciable areas of Bangladesh, near-surface clay sediments, which may be as thin as 2 m, have been removed and piled in order to raise village levels above flood levels and structure rice fields, leaving ponds that, along with irrigation fields, may act as sources of aquifer recharge[37]. At our field site in Cambodia, the clay unit is thicker (up to 20 m) and the majority of people live on natural river levees and therefore the near-surface sediment structure is much less distorted. Perhaps most importantly, low population densities along the Cambodian delta have limited the drive to increase food production through irrigation based on groundwater pumping. This lack of hydrologic disturbance provides an opportunity to evaluate groundwater conditions that predate significant human disturbance and associated complexity.

Supplementary Table 1. Aqueous concentrations from aquifer well, shallow well, and surface water samples collected from November, 2005 – February, 2006.

		Aquifer Wells (n = 48)				**Shallow Wells** (n = 25)				**Surface Water** (n = 24)			
		Min	**Max**	**Average**	**Median**	**Min**	**Max**	**Average**	**Median**	**Min**	**Max**	**Average**	**Median**
As	μg/L	15	1300	500	480	0.00	1000	160	50	0.0	9.8	1.4	0.0
pH		6.3	9.1	7.1	7.1	6.5	7.4	6.8	6.7	6.2	7.6	6.8	6.8
Eh	mV	-190	290	70	41	-86	350	110	140	240	450	310	310
TDS	μS/cm	43	2300	1100	1100	100	3900	1600	1800	11	230	130	130
DO	mg/L	< 1	1.4	< 1	< 1	< 1	2.0	< 1	< 1	< 1	7.5	3.7	3.6
Al	mg/L	< 0.01	0.03	< 0.01	< 0.01	< 0.01	< 0.01	< 0.01	< 0.01	< 0.01	0.15	0.03	< 0.01
Ca	mg/L	22	130	71	65	60	290	130	110	11	27	19	19
K	mg/L	0.88	9.3	3.8	3.2	0.27	36	4.2	1.9	0.20	4.0	1.9	1.8
Fe	mg/L	0.00	24	8.0	8.0	0.0	26	4.0	2.3	0.0	0.37	0.08	0.04
Mg	mg/L	8.7	43	24	22	16	120	51	43	2.5	8.1	4.6	4.5
Mn	mg/L	0.01	3.2	0.79	0.55	0.00	4.9	1.6	1.5	0.00	0.38	0.05	0.03
Na	mg/L	8.4	110	44	43	12	210	83	74	2.4	8.9	5.7	5.7
P	mg/L	0.04	4.2	1.2	0.91	0.04	1.9	0.49	0.20	0.00	0.09	0.02	0.02
S	mg/L	0.47	22	2.4	1.4	1.5	160	28	18	0.59	1.7	0.97	0.99
Si	mg/L	5.3	37	17	13	7.6	30	16	15	2.3	7.0	5.2	5.4
F^-	mg/L	< 0.3	1.0	<0.3	<0.3	< 0.3	1.5	< 0.3	< 0.3	< 0.3	< 0.3	< 0.3	< 0.3
Cl^-	mg/L	3.5	160	19	9.1	5.2	340	110	58	2.4	9.9	5.9	5.8
PO_4^{3-}	mg/L	< 0.4	13	3.2	2.7	< 0.4	5.6	1.1	< 0.4	< 0.4	< 0.4	< 0.4	< 0.4
SO_4^{2-}	mg/L	< 0.5	58	8.2	5.6	4.7	440	76	52	0.84	3.8	2.0	2.0
NO_3-N	mg/L	< 0.02	0.08	0.03	0.03	< 0.02	15	2.8	0.10	< 0.02	0.06	0.01	< 0.02
NH_4-N	mg/L	1.6	84	20	13	0.75	29	6.4	1.4	0.72	0.88	0.80	0.80
DOC	mg/L	1.0	24	6.9	5.2	0.09	19	3.3	2.2	2.2	7.1	4.4	4.6
Alkalinity	mg/L $CaCO_3$	200	760	420	420	210	860	530	480	39	96	67	69
Sulfide	μg/L	< 1	96	7.4	2.7	< 1	19	2.2	1.0	NA	NA	NA	NA

3. Water levels and flux calculations

Mekong River stage levels are provided by the Mekong River Commission and are representative of the recent historical average. Local hydraulic gradients between rivers and the adjacent wetland and underlying floodplain aquifer are two-orders of magnitude greater than the regional gradient extending parallel with the river towards the ocean, indicating the flow direction is perpendicular to the Mekong River. Importantly, differences in hydraulic head both horizontally and vertically are typically on the scale of decimeters to meters, while our measurement error was sub-centimeter, providing a high degree of certainty for the net gradient calculations. Additionally, the average annual head of the ponds/wetlands is 1.4 m higher than that of the rivers; between those monitoring points, our maximum surveying error (based on completion of surveying circles) is 0.9 cm. Thus our surveying error is less than 1% of the average annual head difference.

While the relative elevations of the wetlands and the river levels invert semi-annually (Figure 1 in main text, Supplementary Figure 2, and Supplementary Figure 3), the wetlands are higher than the river for 9 out of the 12 months of the year. The measured gradients provide an internally consistent driving force for steady-state mass balance of water flux downwards from the wetlands and horizontally from the aquifer to the river. Hydraulic data from a site in the Munshiganj district of Bangladesh illustrate similar patterns to those observed here for the Mekong Delta for two months after wet season floods, but upon initiation of dry season groundwater pumping, aquifer water levels fall below those of the river, altering groundwater flow[37].

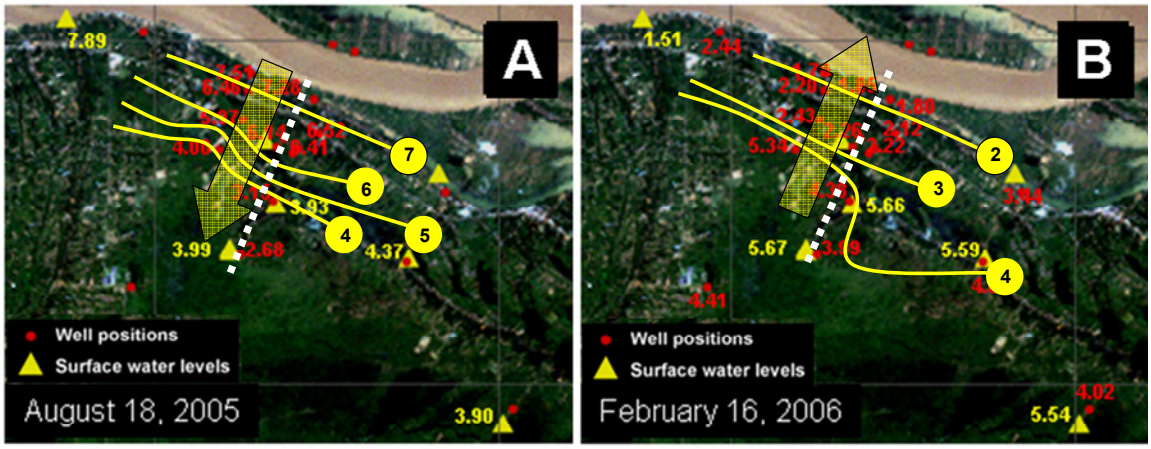

Supplementary Figure 2. Map view of hydraulic heads in wells and surface waters on August 18, 2005 and February 16, 2006, illustrating seasonal shifts in gradients. Red numbers indicate heads in medium depth aquifer wells (20-30 m) and yellow numbers represent surface water hydraulic heads (all reported in MASL). White dotted lines indicate cross-section traces for Supplementary Figure 4. Yellow lines and circled numbers indicate hand contoured lines of equipotential and yellow arrows denote flow directions. (A) During the wet season gradients indicate flow from the Mekong River to the wetlands. (B) During the dry season, flow reverses.

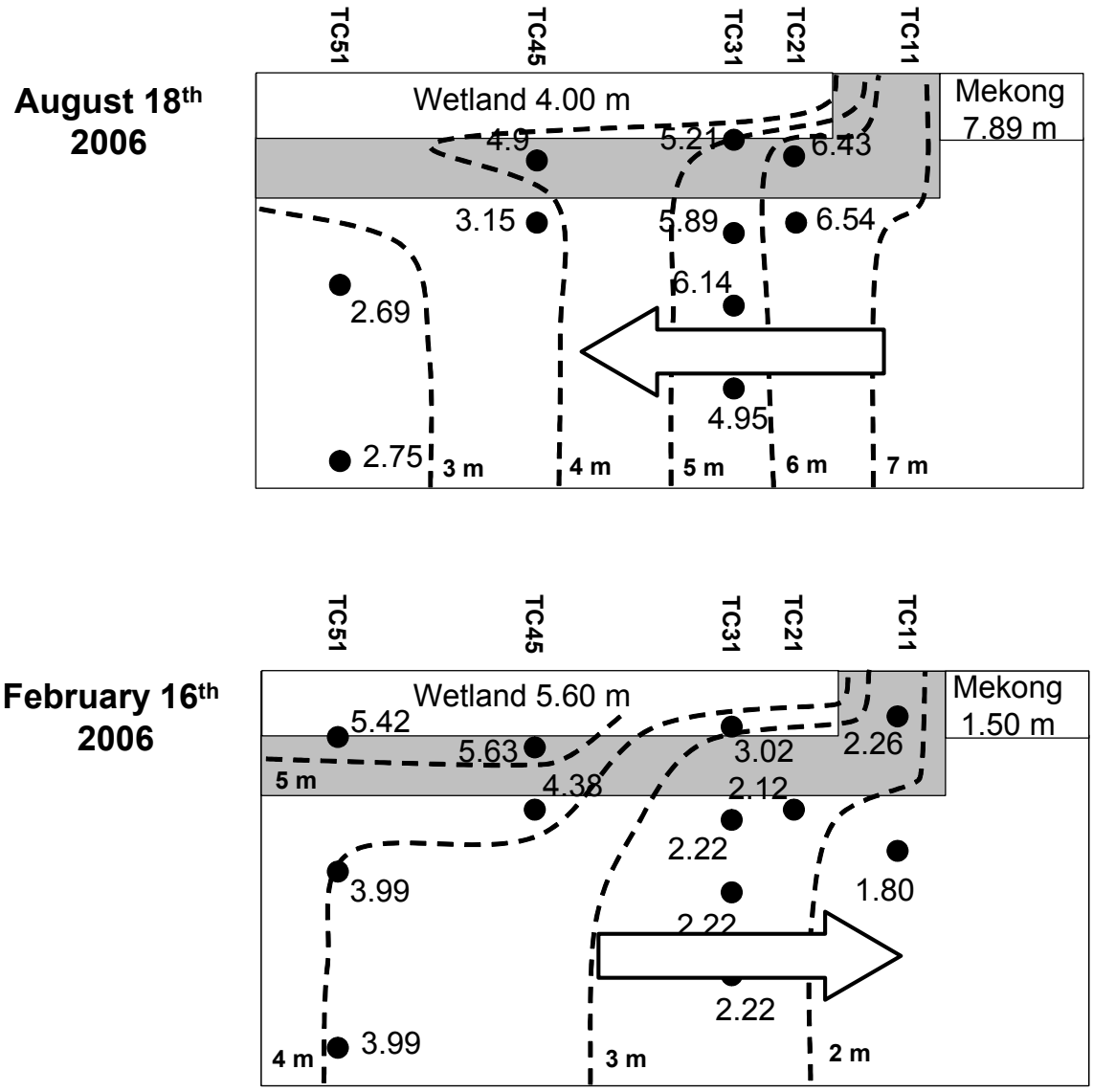

Supplementary Figure 3. **Cross-sectional view (along transect depicted in Supplementary Figure 2) of hydraulic heads in wells and surface waters on August 18, 2005 and February 16, 2006, illustrating seasonal shifts in gradients.** Black circles indicate well screen locations, associated values are in MASL. Dashed lines indicate hand contoured lines of equal potential Note that despite the vertical exaggeration, cross-sections are to scale.

We performed field and laboratory investigations to determine hydraulic conductivities (Supplementary Table 2). For the upper clay sediments, falling head and rising head slug tests were performed in the field for 15 shallow wells. Fine-grained sediments were also collected (for locations, see Figure 1, main text) for laboratory constant-head permeameter tests, and median values were used to calculate groundwater fluxes. In-field slug tests and laboratory permeameter tests result in hydraulic conductivities of the clay unit ranging from approximately 10^{-8} to 10^{-7} m s^{-1}. The hydraulic conductivity of the sand

aquifer unit was determined by particle size analyses and resulting K values range from approximately 10^{-4} to 10^{-3} m s^{-1} (Supplementary Table 2).

We used annual gradients between the ponds and three wells to determine vertical flow distances (Supplementary Table 3). Assuming a porosity of 0.5[32], net annual vertical flow distances are 0.04 to 0.4 m from the wetland-ponds to the aquifer. If groundwater recharge is evenly distributed across our entire field area (~50 km^2), annual downward fluxes range from $2x10^6$ to $2x10^7$ m^3 y^{-1}. Due to the symmetry of our field area (i.e. it is bounded by the Mekong and Bassac Rivers), the range of downward fluxes that discharge to each river is 10^6 to 10^7 m^3 y^{-1}.

We used 5 annual gradients between wells and the Mekong River to determine annual horizontal groundwater flow distances. Assuming a porosity of 0.2[32], net annual horizontal groundwater flow to the river ranges from 1.3 to 13 m. In order to calculate groundwater fluxes, we employed a vertical surface parallel to the river with a thickness of 50 m (an approximate aquifer thickness). Given our field area width of ~6 km, the net annual horizontal groundwater flux within the aquifer towards the Mekong River ranges from $4x10^5$ to $4x10^6$ m^3 y^{-1}.

The results obtained here are supported by the fact that average annual pond/wetland hydraulic heads are 1.4 m higher than average annual river heads; thus groundwater flow is expected from the wetlands through the aquifer and to the river. This trend in groundwater flow is similar to model-predicted results for the Bangladeshi aquifer without groundwater pumping[37]. Additionally, groundwater modeling produced an idealized flow solution, calibrated to observed hydraulic trends, that is consistent with the mass balance calculations shown above (see discussion below).

Supplementary Table 2. Summary results of hydraulic conductivity determination for aquifer sand and surface clay sediments.

	Aquifer sands	Surface clays	
Method	**Grain size**	**Permeameters**	**Slug tests**
Average K (m/s)	3.15E-04	4.08E-07	1.22E-06
Standard deviation (m/s)	3.02E-04	5.94E-07	1.89E-06
Median K (m/s)	2.70E-04	5.02E-08	4.76E-07
Number of samples	14	10	15

Supplementary Table 3. Net annual groundwater flow distances.

	Vertical flow		Horizontal flow	
	Minimum ($K=10^{-8}$ m/s)	**Maximum ($K=10^{-7}$ m/s)**	**Minimum ($K=10^{-4}$ m/s)**	**Maximum ($K=10^{-3}$ m/s)**
Average net yearly flow distance (m)	0.04	0.43	1.3	12.8
Standard deviation (m)	0.003	0.034	0.87	8.78
Number of calculations	3	3	5	5

4. Groundwater flow modeling

Numerical modeling was conducted using MODFLOW and MODPATH[38] under both transient and steady-state (net annual) conditions. Simulations were conducted in a two dimensional cross-sectional grid (60 m, 20 cell depth; 4000 m, 400 cell width, Supplementary Figure 5). An assumption of symmetry between the Bassac and Mekong Rivers enables the establishment of a no flow boundary at the center of the wetlands and the middle of the Mekong River. The base of the aquifer (e.g. contact with underlying bedrock, assumed to be at 60 m) is also assigned a no flow boundary condition. Transient boundary conditions based on measured water levels over the time period from January 2005 to March 2006 (Figure 1, main text) are assigned to the river and wetlands. These boundary conditions are represented by cells 9 m thick to accommodate seasonal head fluctuations. The hydraulic conductivity field is expressed as a simplified 2-layer system with 13 m of clay overlying 38 m of sand. Material properties were fixed based on field and literature values (Supplementary Table 4) with the exception of hydraulic conductivity values, which were treated as the primary variables during transient model calibration. Hydraulic conductivity values were constrained by the range of field-measured values and by the field-expressed ratio in gradients across the clay and sand, respectively.

Model calibration was conducted by adjusting hydraulic conductivity values for the clay and sand to reproduce field-observed temporal trends (both seasonal and daily tidal) in hydraulic head values in wells at varying distances from the Mekong River (Supplementary Figures 5A-C). The assumption of 2-dimensionality (i.e. all flow perpendicular to the river) was validated by confirming that the model results also matched results along parallel well transects (Supplementary Figure 5B). The resulting hydraulic conductivity values were used in steady-state (annual average) flow simulations in which the wetland and river heads were fixed to produce the observed average annual head difference; this output is plotted in Figure 3 (main text) and Supplementary Figure 4.

The modeling results quantitatively validate the presented mass balance calculations. The simulated results, using a highly idealized 2-dimensional, two-layer K distribution (clay and sand), exhibit a remarkably good fit to observed seasonal and daily-tidal trends. At select locations (e.g. TC45) the simulation results do not match observed trends, highlighting the importance of local hydraulic complexity in dictating local flow behavior.

Importantly, uncertainty in aquifer storativity and hydraulic conductivity values preclude the use of the flow modeling to markedly improve estimate of aquifer residence times. However, the simulated flow lines are independent of storativity values and are primarily constrained by the ratio of clay to sand hydraulic conductivity (a ratio well constrained within the simulations). Therefore, the flow lines plotted in Figure 3 (main text) and Supplementary Figure 4 provide a sound estimate of the net seasonal flow direction.

Supplementary Table 4. Material properties used in net annual model simulations

	River	Wetland	Sand	Clay
Fixed Parameters				
Specific storage(m^{-1})^	0	5×10^{-4}	1×10^{-4}	5×10^{-4}
Porosity#	1	0.5	0.2	0.5
Calibrated Parameters				
Horizontal K ($m\ sec^{-1}$)*	1	1×10^{-8}	3.5×10^{-4}	1×10^{-8}
Vertical K ($m\ sec^{-1}$)*	1	1×10^{-8}	3.5×10^{-4}	1×10^{-8}

^ Based on literature values[39,40,41,42]
# Based on literature values[32]
* Derived from transient model calibration

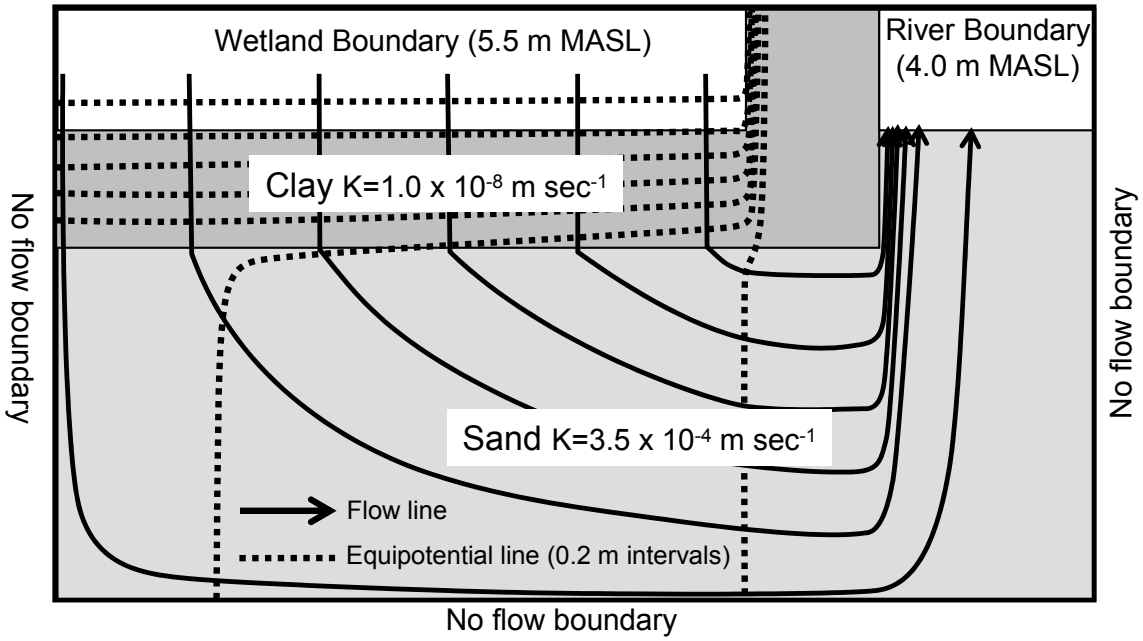

Supplementary Figure 4. Model domain and output of idealized net annual flow field.

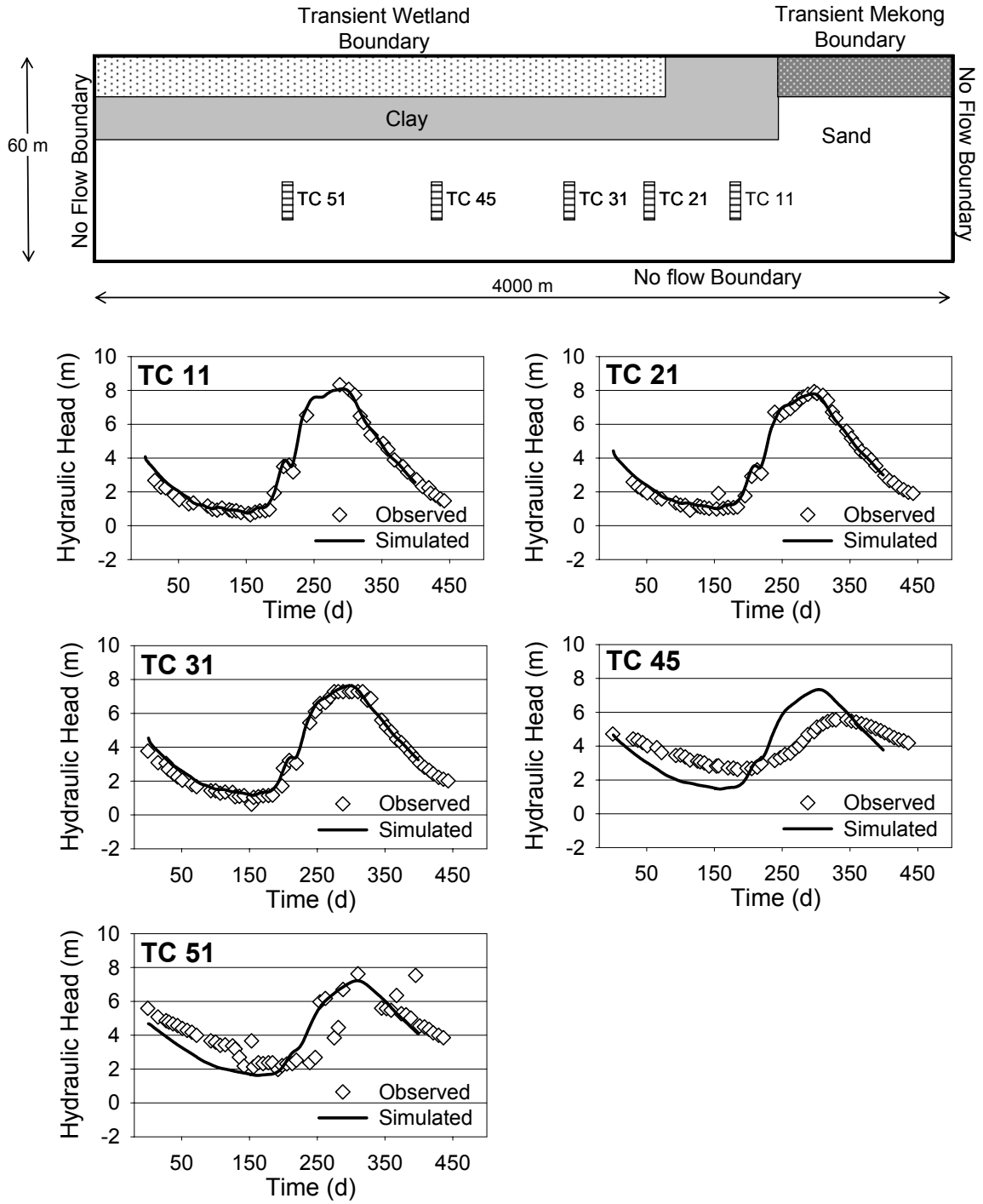

Supplementary Figure 5a. **Model calibration results to the TC well transect.** Deviations from observed values for later time data in TC51 and TH71 (Supplementary Figure 6b) likely reflects field measurement error. However, deviations from observed values for Well TC45 as well as early time data at TC51 and TH71 likely reflect real differences between the field conditions and the highly idealized system represented by the model. Specifically, the poor fit for these data appear to indicate greater influence from the wetlands at these locations, suggesting that the clay may be thinner, or more conductive, at these sites.

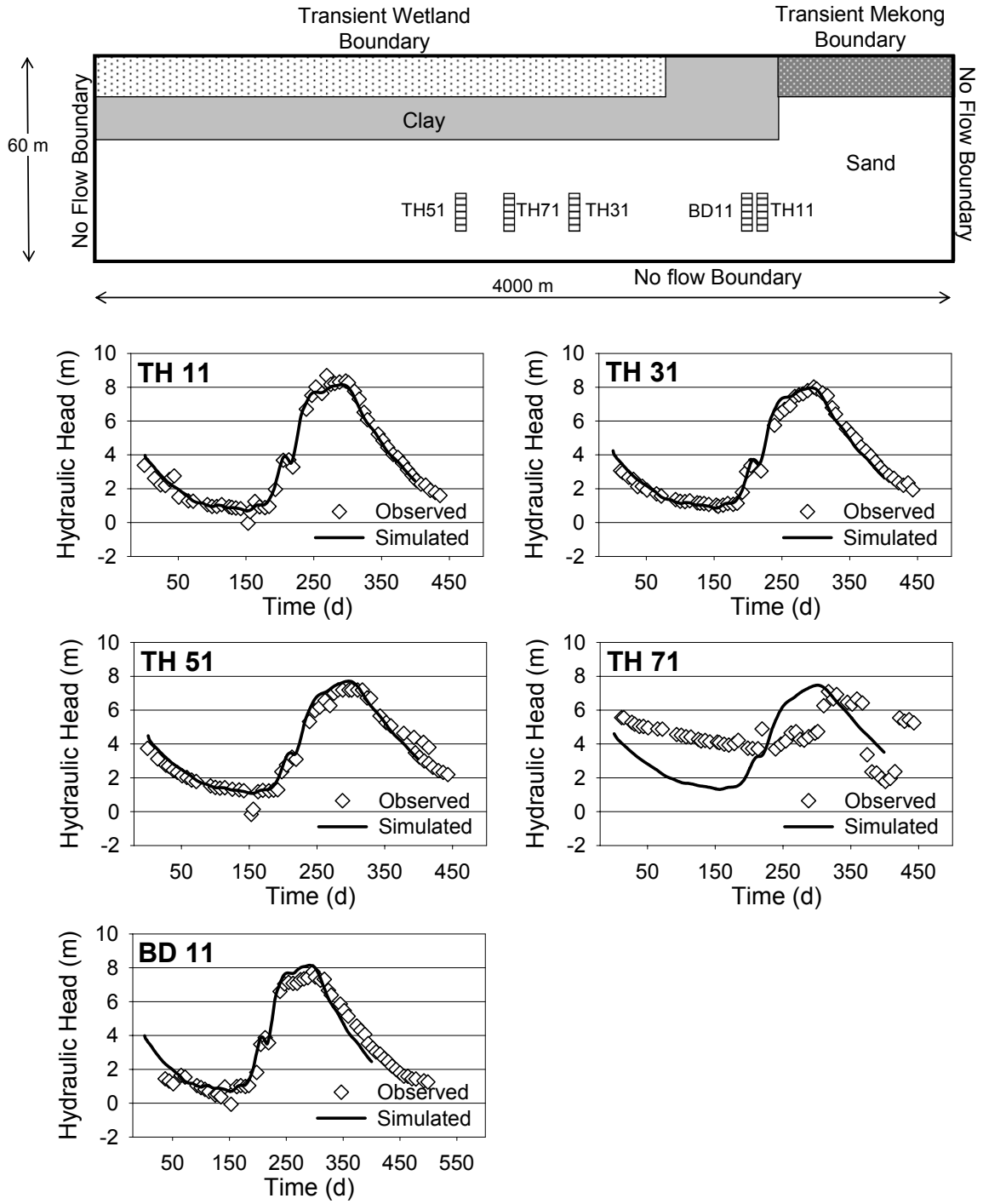

Supplementary Figure 5b. Model calibration results to the TH and BD well transects. Deviations from observed values for later time data in TC51(Supplementary Figure 6a) and TH71 likely reflects field measurement error. However, deviations from observed values for Well TC45 as well as early time data at TC51 and TH71 likely reflect real differences between the field conditions and the highly idealized system represented by the model. Specifically, the poor fit for these data appear to indicate greater influence from the wetlands at these locations, suggesting that the clay may be thinner, or more conductive, at these sites.

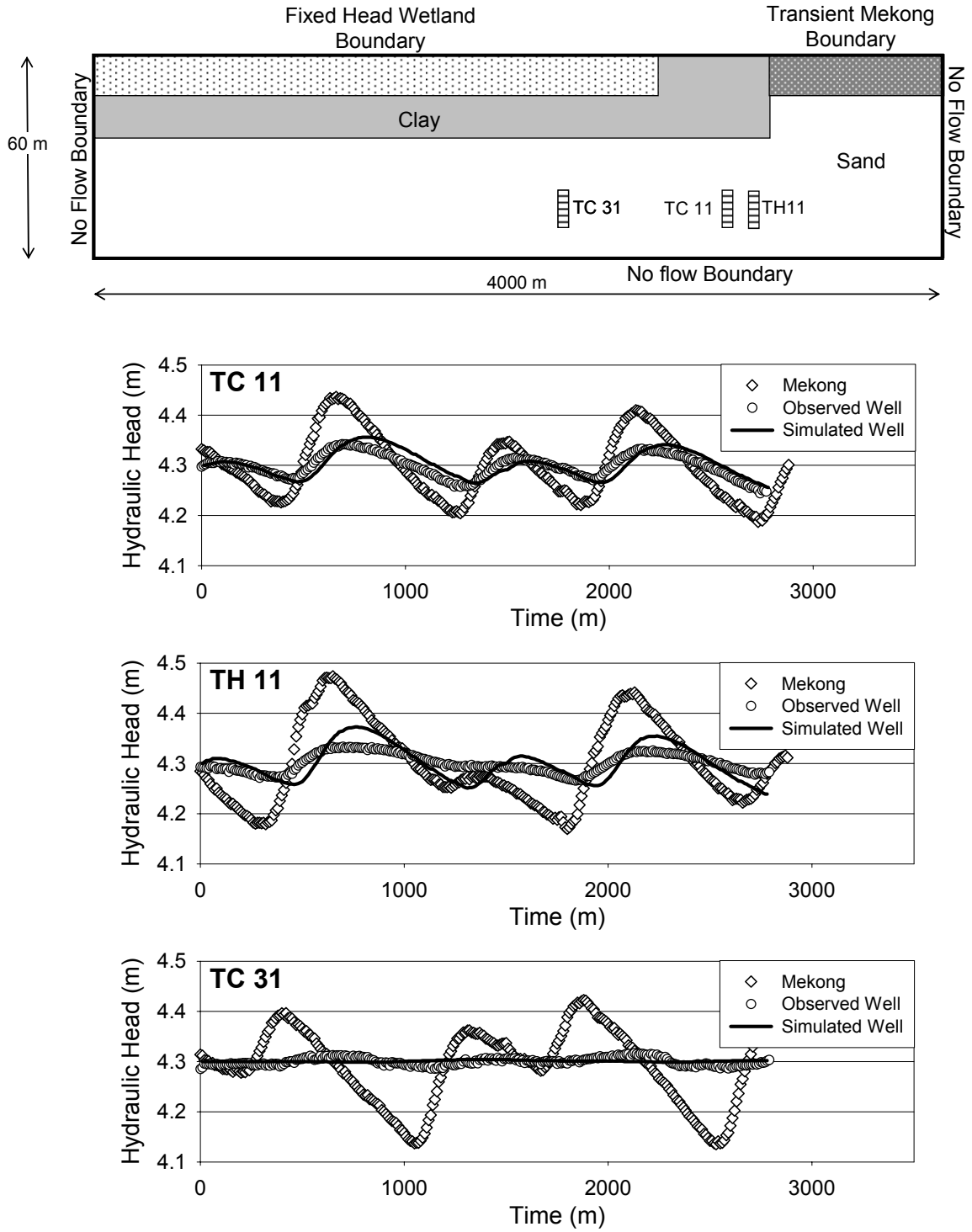

Supplementary Figure 5c. **Model calibration results to tidal fluctuations at TC11, TH11 and TC31.** Each simulation was performed with the plotted Mekong data as a transient boundary condition and a fixed head wetland boundary.

5. Dissolved and solid-phase arsenic

Dissolved arsenic concentrations vary spatially across the aquifer (average: 500 μg L^{-1}; range: 15-1300 μg L^{-1}) (Supplementary Table 1), and there are only modest increases in arsenic along the flow path to the aquifer-river boundary zone. The highest dissolved arsenic concentrations are observed immediately below (~20 m depth) present-day abandoned river channel ponds, and concentrations of >900 μg L^{-1} trend downward towards deeper (40-57 m) wells adjacent to the Mekong River (Figures 2 and 3, main text, and discussion below), where aquifer sediments are often coarser than the typical fine sands, and at depths from where pebbles up to 1 cm in diameter have been recovered.

Individual arsenic concentrations measured for each well and each sampling time point are presented in the table in the Appendix of the Supplementary Information.

Shallow wells (0-13 m) in our field area typically have As concentrations < 100 μg L^{-1}. An exception is the shallow wells adjacent to old river channel ponds and our shallow well in the middle of the wetlands (Supplementary Figure 6). Although concentrations vary seasonally and shallow wells are typically screened across the water table, concentrations reach 460 μg L^{-1}. Lysimeter and discretely-screened shallow wells in the ponds have As concentrations as high as 700 μg L^{-1} at 8 m depth, a value approaching the As concentrations in the aquifer sands that trend towards the Mekong River.

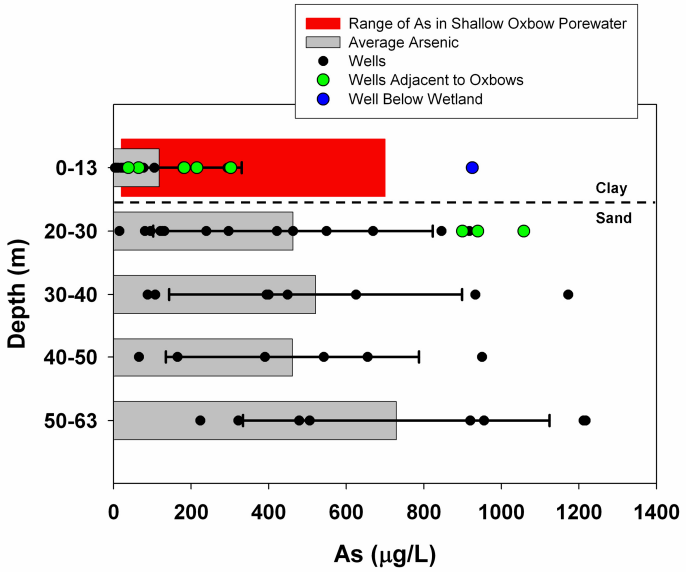

Supplementary Figure 6. Arsenic concentrations from wells binned by depth for all wells between the central wetlands and Mekong River. For each individual well, As concentrations from each sampling between March 2005 and March 2006 were averaged. These averages are depicted by the black, green, and blue dots. All values for each bin depth of arsenic well water concentrations were then averaged and are depicted by the thick grey bars, with error bars indicating standard deviations of the concentrations in the depth bins. Thus, each bin incorporates 15-37 individual measurements. The range of As concentrations measured in shallow porewater (wells and lysimeters) adjacent to old river channel ponds (oxbows) is represented by the red bar.

Within our detailed field area, the highest well water arsenic concentrations occur between the old river channel ponds and the Mekong River (Supplementary Figure 7).

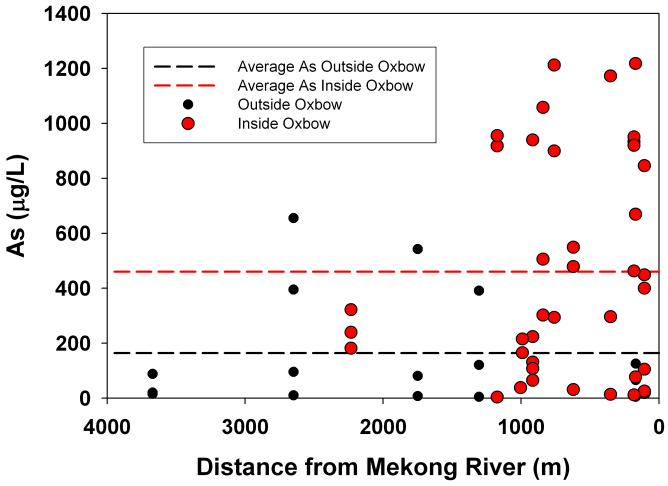

Supplementary Figure 7. Arsenic concentrations in relation to old river channel (oxbow) ponds within our detailed study area. The average arsenic concentrations for the two groups are indicated by the horizontal dotted lines. Individual well concentrations are plotted as dots.

At equivalent distances from the Mekong River (i.e. such that pond-river distances are normalized along a transect perpendicular to the river), arsenic concentrations are comparable within our detailed field area. Thus a cross-section of dissolved arsenic concentrations reveals that the highest arsenic concentrations trend downward from the ponds towards the Mekong River, as shown in Figures 2 and 3 of the main text.

Seasonal trends in arsenic concentrations are observed at multiple wells adjacent to the Mekong River (Supplementary Figure 8A). In near-river wells, arsenic concentrations decline during periods of river-to-aquifer flow and are highest during aquifer-to-river flow highlighting the mobility of dissolved arsenic within the aquifer, a finding consistent with laboratory incubations of Bangladesh sediments[43] as well as the enhanced mobility of As(III) under flow conditions[44]. Changes in arsenic are positively correlated with changes in dissolved NH_4^+ and negatively correlated with SO_4^{2-}.

Recharge zone pore water arsenic concentrations are highest when steep downward gradients induce water flow into the underlying aquifer, indicative of reductive arsenic release from the most shallow surficial sediments during seasonal saturation. Within near-surface porewater (Supplementary Figure 8B), dissolved Fe(II) concentrations follow arsenic, while SO_4^{2-} concentrations are inversely correlated, suggesting changing redox conditions.

Solid-phase arsenic concentrations are ~12 mg Kg^{-1} in the oxidized layers of surficial clays, and decrease in the deeper (>3 m) grey clays. In the sandy aquifer sediments, solid-phase arsenic concentrations average ~3 mg Kg^{-1} and are relatively spatially uniform.

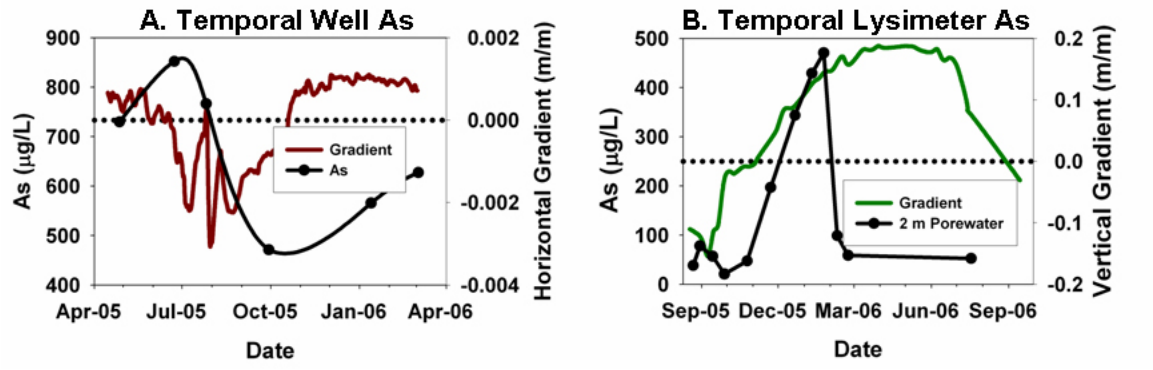

Supplementary Figure 8. Temporal variations in arsenic concentrations following shifting hydrologic gradients. (A) In the aquifer, arsenic concentrations vary by as much as 50% in wells adjacent to the Mekong River (e.g. TC11-25 shown here). Concentrations rise when aquifer horizontal gradients are positive, indicating flow towards the river, and decrease during inflow from the river. (B) In the near-surface porewaters from lysimeter samples, arsenic concentrations rise as vertical hydraulic gradients change from upward flow (negative gradients) to downward flow (positive gradients).

Typical solid-phase As concentrations are below limits required for bulk speciation techniques. Accordingly, we used micro-X-ray absorption near-edge structure (µ-XANES) spectroscopy to determine the As speciation within the sediments (Supplementary Figure 9). In the upper surface sediments (10 cm), As exists predominantly as arsenate, but with increasing depth, arsenite dominates the solid-phase speciation. Additionally, the deeper reduced sediments also contain As-bearing sulfide grains. These results indicate reduction of As with depth.

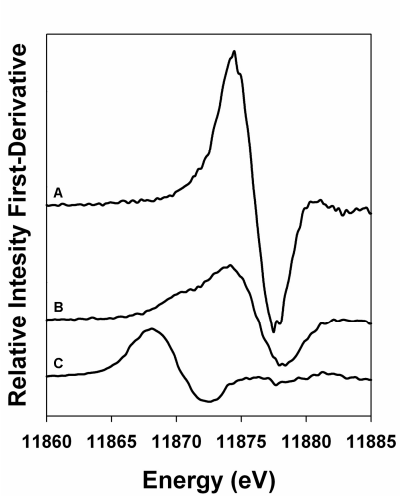

Supplementary Figure 9. First-derivative XANES of near-surface sediments from site adjacent to old river channel ponds. (A) 10 cm depth sediments show As predominantly as arsenate (As(V)). (B) 4 m depth sediments show a mixture of arsenite (As(III)) and arsenate (As(V)). (C) In 4 m sediments, As is also found associated with sulfides in individual sediment As "hotspots".

6. Arsenic inputs and outputs

6a. Inputs via sedimentation

Our ^{14}C dates indicate that the bottom-most clay layers of the near-surface sediments are $\geq$6000 years old. Throughout our field area, total clay thicknesses range from 6-20 m. Thus our range of yearly sedimentation is:

6 m / 6000 y x 1000 mm/m = 1 mm/y sedimentation
20 m / 6000 y x 1000 mm/m = 3.3 mm/y sedimentation

Our field area is ~50 km^2. Therefore, assuming a porosity of 0.5 in the clay sediments and a solid-phase density of quartz (2.65 g/cm^3), the range of masses of sediments deposited over our field area annually is:

50 km^2 x 1 mm/y x 0.5 x 2.65 g/cm^3 x $(10^5$ cm/km$)^2$ x 0.1 cm/mm = $6.6x10^{10}$ g/y
50 km^2 x 3.3 mm/y x 0.5 x 2.65 g/cm^3 x $(10^5$ cm/km$)^2$ x 0.1 cm/mm = $2.2x10^{11}$ g/y

The uppermost clay sediments have solid-phase As concentrations of ~12 μg/g and the lowermost clays and aquifer sands have As concentrations of ~3 μg/g. Therefore, if As concentrations have remained constant during deposition, 9 μg/g of As may be mobilized.

Therefore, the range of mobilizable As deposited over our field area annually is:

$6.6x10^{10}$ g/y x 9 μg/g = $6x10^{11}$ μg As/y
$2.2x10^{10}$ g/y x 9 μg/g = $2x10^{12}$ μg As/y

6b. Outputs via groundwater discharge

The net annual horizontal flux between the aquifer and river ranges from $4x10^5$ m^3/y to $4x10^6$ m^3/y (see Supplementary Information Section 3). Given an As concentration of 500 μg/L, the yearly quantity of As discharged to the Mekong over our field area is:

$4x10^5$ m^3/y x 10^6 cm^3/m^3 x 1 mL/cm^3 x 1 L/1000 mL x 500 μg/L = $2x10^{11}$ μg As
$4x10^6$ m^3/y x 10^6 cm^3/m^3 x 1 mL/cm^3 x 1 L/1000 mL x 500 μg/L = $2x10^{12}$ μg As

Because our field area is symmetrical, As is discharged to both the Mekong and Bassac Rivers and the range of total As discharged is:

$2x10^{11}$ μg As x 2 = $4x10^{11}$ μg As
$2x10^{12}$ μg As x 2 = $4x10^{12}$ μg As

7. Supporting information references

30. *Method 3052: Microwave assisted acid digestion of siliceous and organically based matrices,* 3rd ed.; U.S. Environmental Protection Agency: Washington, DC, Vol. 2004 (1994).
31. Kresic, N. *Quantitative Solutions in Hydrogeology and Groundwater Modeling*. CRC, Boca Raton. 480 p (1997).
32. Domenico, P. A. & Schwartz, F. W. *Physical and Chemical Hydrogeology*. John Wiley & Sons, New York. 506 p (1998).
33. Hvorslev, M. J. *Time lag and soil permeability in groundwater observations.* U.S. Army Corps of Engineers Waterway Experimentation Station, Bulletin 36, Vicksburg, Miss (1951).
34. Nguyen, V. L., Ta, T. K. O. & Tateishi, M. Late Holocene depositional environments and coastal evolution of the Mekong River Delta, Southern Vietnam. *J. Asian Earth Sci.* **18**, 427-439 (2000).
35. Ta, T. K. O. et al. Holocene delta evolution and sediment discharge of the Mekong River, southern Vietnam. *Quaternary Sci. Rev*. **21**, 1807-1819 (2002).
36. Tamura, T. *et al*. Depositional facies and radiocarbon ages of a drill core from the Mekong River lowland near Phnom Penh, Cambodia: Evidence for tidal sedimentation at the time of Holocene maximum flooding. *J. Asian Earth Sci.* **29**, 585-592 (2007).
37. Harvey, C. F. *et al*. Groundwater dynamics and arsenic contamination in Bangladesh. *Chem. Geo.* **228**, 112-136 (2006).
38. McDonald, M.G., & Harbaugh, A.W. A modular three-dimensional finite-difference ground-water flow model. *U.S. Geological Survey Techniques of Water-Resources Investigations.* Book 6, Chap. A1, 586 p (1988).
39. Fleckenstein, J. H., Niswonger, R. G. & Fogg, G. E. River-aquifer interactions, geologic heterogeneity, and low-flow management. *Ground Water* **44**, 837-852 (2006).
40. Konikow, L. F. & Neuzil, C. E. A method to estimate groundwater depletion from confining units. Water Resources Research, **43**, 1-14 (2007).
41. Masterson, J. P. & Barabedian, S. P. Effects of sea-level rise on ground water flow in a coastal aquifer system. *Ground Water* **45,** 209-217 (2007).
42. Thangarajan, M., Linn, F., Uhl, V., Bakaya, T.B., Gabaake, G.G. Modeling an inland delta aquifer system to evolve pre-development management schemes: a case study in Upper Thamalakane river valley, Botswana, southern Africa. *Environmental Geology*, **38**, 285-295 (1999).
43. Polizzotto, M. L., Harvey, C. F., Sutton, S. R. & Fendorf, S. Processes conducive to the release and transport of arsenic into aquifers of Bangladesh. *Proc. Nat. Acad. Sci.U. S. A.* **102**, 18819-18823 (2005).
44. Kocar, B. D., Herbel, M. J., Tufano, K. J. & Fendorf, S. Contrasting effects of dissimilatory iron(III) and arsenic(V) reduction on arsenic retention and transport. *Environ. Sci. Technol.* **40**, 6715-6721 (2006).

Appendix: As well data

Well site	Depth (m)	UTM x (m)	UTM y (m)	Date sampled	As (μg/L)
BD11-12	12	500572	1267749	4/29/2005	8
BD11-12	12	500572	1267749	12/14/2005	40
BD11-20	20	500572	1267749	4/29/2005	11
BD11-47	47	500572	1267749	4/29/2005	74
BD11-47	47	500572	1267749	12/14/2005	116
BD31-12	12	500459	1268232	5/4/2005	276
BD31-12	12	500459	1268232	12/25/2005	143
BD31-20	20	500459	1268232	5/4/2005	214
BD31-20	20	500459	1268232	12/20/2005	225
BD31-49	49	500459	1268232	5/9/2005	145
BD31-49	49	500459	1268232	12/15/2005	140
BD51-12	12	500568	1268700	5/10/2005	39
BD51-12	12	500568	1268700	1/4/2006	67
BD51-20	20	500568	1268700	5/10/2005	164
BD51-20	20	500568	1268700	1/4/2006	178
BD51-30	30	500568	1268700	5/11/2005	261
BD51-30	30	500568	1268700	12/29/2005	264
MI11-12	12	502587	1274945	11/28/2005	47
MI11-25	25	502587	1274945	11/29/2005	514
MI11-34	34	502587	1274945	11/28/2005	770
MI12-12	12	502905	1274841	11/30/2005	39
MI12-25	25	502905	1274841	11/29/2005	1034
MI12-36	36	502905	1274841	11/30/2005	1268
PE21-12	12	504222	1272797	2/14/2006	4
PE21-25	25	504222	1272797	2/15/2006	918
PE21-63	63	504222	1272797	2/14/2006	955
PE31-9	9	503659	1271776	2/22/2006	181
PE31-25	25	503659	1271776	2/7/2006	239
PE31-60	60	503659	1271776	2/22/2006	322
PE51-12	12	505204	1269637	2/28/2006	925
PE51-25	25	505204	1269637	2/27/2006	421
PE51-40	40	505204	1269637	2/28/2006	625
PE71-12	12	503694	1267715	2/21/2006	47
PE71-25	25	503694	1267715	2/20/2006	345
PE71-52	52	503694	1267715	2/21/2006	165
PW11-12	12	499836	1275129	2/13/2006	5
PW11-25	25	499836	1275129	2/8/2006	125
PW11-43	43	499836	1275129	2/13/2006	66
PW31-12	12	499657	1271421	2/6/2006	20
PW31-25	25	499657	1271421	2/7/2006	15
PW31-33	33	499657	1271421	2/6/2006	88
PW51-12	12	497425	1267363	1/30/2006	54
PW51-25	25	497425	1267363	1/31/2006	1071
PW51-47	47	497425	1267363	1/30/2006	16
TC11-9	9	502313	1274145	6/23/2005	96

TC11-9	9	502313	1274145	9/29/2005	49
TC11-9	9	502313	1274145	1/12/2006	88
TC11-9	9	502313	1274145	3/1/2006	85
TC11-9	9	502313	1274145	5/17/2006	67
TC11-9	9	502313	1274145	6/16/2006	49
TC11-9	9	502313	1274145	8/8/2006	16
TC11-9	9	502313	1274145	9/15/2006	10
TC11-9	9	502313	1274145	11/14/2006	40
TC11-9	9	502313	1274145	12/20/2006	80
TC11-9	9	502313	1274145	1/16/2007	78
TC11-9	9	502313	1274145	2/1/2007	98
TC11-9	9	502313	1274145	2/26/2007	92
TC11-25	25	502313	1274145	4/27/2005	730
TC11-25	25	502313	1274145	6/23/2005	852
TC11-25	25	502313	1274145	7/26/2005	766
TC11-25	25	502313	1274145	9/29/2005	471
TC11-25	25	502313	1274145	1/13/2006	566
TC11-25	25	502313	1274145	3/3/2006	627
TC11-25	25	502313	1274145	5/3/2006	671
TC11-25	25	502313	1274145	6/14/2006	693
TC11-25	25	502313	1274145	7/26/2006	645
TC11-25	25	502313	1274145	9/19/2006	463
TC11-25	25	502313	1274145	11/14/2006	500
TC11-25	25	502313	1274145	12/7/2006	522
TC11-25	25	502313	1274145	1/16/2007	571
TC11-25	25	502313	1274145	1/25/2007	602
TC11-25	25	502313	1274145	2/21/2007	623
TC11-57	57	502313	1274145	4/28/2005	1149
TC11-57	57	502313	1274145	6/24/2005	1288
TC11-57	57	502313	1274145	7/25/2005	1232
TC11-57	57	502313	1274145	9/30/2005	1180
TC11-57	57	502313	1274145	1/12/2006	1002
TC11-57	57	502313	1274145	3/1/2006	1304
TC11-57	57	502313	1274145	5/12/2006	1366
TC11-57	57	502313	1274145	6/16/2006	1299
TC11-57	57	502313	1274145	8/9/2006	1071
TC11-57	57	502313	1274145	9/12/2006	1050
TC21-12	12	502389	1273654	11/8/2005	31
TC21-20	20	502389	1273654	4/4/2005	557
TC21-20	20	502389	1273654	11/8/2005	541
TC21-51	51	502389	1273654	4/5/2005	479
TC21-51	51	502389	1273654	11/8/2005	478
TC31-8	8	502085	1273436	3/10/2005	35
TC31-8	8	502085	1273436	8/16/2005	85
TC31-8	8	502085	1273436	10/17/2005	60
TC31-8	8	502085	1273436	1/25/2006	78
TC31-8	8	502085	1273436	12/5/2006	65
TC31-8	8	502085	1273436	1/17/2006	121

TC31-8	8	502085	1273436	2/5/2007	139
TC31-20	20	502085	1273436	3/8/2005	945
TC31-20	20	502085	1273436	6/27/2005	962
TC31-20	20	502085	1273436	8/16/2005	873
TC31-20	20	502085	1273436	10/17/2005	984
TC31-20	20	502085	1273436	1/23/2006	934
TC31-20	20	502085	1273436	March, 2006	937
TC31-20	20	502085	1273436	11/28/2006	943
TC31-20	20	502085	1273436	1/18/2007	927
TC31-20	20	502085	1273436	2/7/2007	954
TC31-30	30	502085	1273436	10/18/2005	137
TC31-30	30	502085	1273436	1/25/2006	115
TC31-30	30	502085	1273436	March, 2006	141
TC31-30	30	502085	1273436	12/6/2006	102
TC31-30	30	502085	1273436	1/22/2007	103
TC31-30	30	502085	1273436	2/12/2007	95
TC31-40	40	502085	1273436	10/18/2005	109
TC31-40	40	502085	1273436	1/24/2006	101
TC31-40	40	502085	1273436	March, 2006	114
TC31-40	40	502085	1273436	12/6/2006	97
TC31-40	40	502085	1273436	1/17/2007	86
TC31-40	40	502085	1273436	2/6/2007	84
TC31-40	40	502085	1273436	2/28/2007	93
TC31-51	51	502085	1273436	3/9/2005	252
TC31-51	51	502085	1273436	6/28/2005	231
TC31-51	51	502085	1273436	8/17/2005	210
TC31-51	51	502085	1273436	10/17/2005	209
TC31-51	51	502085	1273436	1/18/2006	222
TC31-51	51	502085	1273436	March, 2006	219
TC31-51	51	502085	1273436	11/22/2006	186
TC31-51	51	502085	1273436	1/23/2007	157
TC31-51	51	502085	1273436	2/8/2007	189
TC41-8	8	502004	1273363	3/10/2005	38
TC45-12	12	501724	1272670	3/25/2005	11
TC45-12	12	501724	1272670	12/22/2005	3
TC45-12	12	501724	1272670	1/30/2007	5
TC45-12	12	501724	1272670	2/20/2007	7
TC45-20	20	501724	1272670	3/30/2005	99
TC45-20	20	501724	1272670	12/28/2005	63
TC45-20	20	501724	1272670	1/29/2007	17
TC45-20	20	501724	1272670	2/14/2007	9
TC45-50	50	501724	1272670	3/31/2005	590
TC45-50	50	501724	1272670	12/22/2005	494
TC45-50	50	501724	1272670	1/31/2007	477
TC45-50	50	501724	1272670	2/15/2007	495
TC51-9	9	501250	1271887	4/6/2005	8
TC51-9	9	501250	1271887	1/10/2006	11
TC51-9	9	501250	1271887	March, 2006	11

TC51-26	26	501250	1271887	4/6/2005	167
TC51-26	26	501250	1271887	6/21/2005	132
TC51-25	26	501250	1271887	8/15/2005	118
TC51-25	26	501250	1271887	9/26/2005	118
TC51-35	35	501250	1271887	9/27/2005	369
TC51-35	35	501250	1271887	1/9/2006	399
TC51-35	35	501250	1271887	March, 2006	416
TC51-49	49	501250	1271887	4/19/2005	641
TC51-49	49	501250	1271887	6/22/2005	695
TC51-49	49	501250	1271887	7/27/2005	688
TC51-49	49	501250	1271887	9/20/2005	700
TC51-49	49	501250	1271887	1/11/2006	561
TC51-49	49	501250	1271887	March, 2006	646
TE11-12	12	501872	1274279	3/16/2005	12
TE11-12	12	501872	1274279	11/14/2005	12
TE11-20	20	501872	1274279	3/16/2005	445
TE11-20	20	501872	1274279	11/14/2005	480
TE11-35	35	501872	1274279	11/15/2005	933
TE11-44	44	501872	1274279	3/18/2005	947
TE11-44	44	501872	1274279	11/14/2005	954
TE11-55	55	501872	1274279	11/15/2005	920
TE51-12	12	501879	1273584	4/20/2005	148
TE51-12	12	501879	1273584	10/19/2005	457
TE51-20	20	501879	1273584	4/20/2005	1012
TE51-20	20	501879	1273584	10/19/2005	1104
TE51-57	57	501879	1273584	4/21/2005	489
TE51-57	57	501879	1273584	10/19/2005	522
TE61-13	13	501766	1273456	4/22/2005	215
TE61-48	48	501766	1273456	March, 2006	165
TH11-9	9	501401	1274532	11/9/2005	20
TH11-12	12	501401	1274532	3/3/2005	66
TH11-12	12	501401	1274532	11/9/2005	5
TH11-12	12	501401	1274532	11/9/2005	5
TH11-13	13	501401	1274532	11/7/2005	105
TH11-25	25	501401	1274532	3/4/2005	821
TH11-25	25	501401	1274532	11/7/2005	870
TH11-37	37	501401	1274532	3/7/2005	514
TH11-37	37	501401	1274532	7/22/2005	395
TH11-37	37	501401	1274532	10/24/2005	451
TH11-37	37	501401	1274532	1/17/2006	453
TH11-37	37	501401	1274532	March, 2006	430
TH11-37	37	501401	1274532	9/26/2006	407
TH11-37	37	501401	1274532	11/15/2006	416
TH11-37	37	501401	1274532	1/15/2007	429
TH11-37	37	501401	1274532	1/24/2007	422
TH11-40	40	501401	1274532	March, 2006	400
TH31-12	12	501357	1274269	3/25/2005	14
TH31-12	12	501357	1274269	10/21/2005	406

TH31-21	21	501357	1274269	3/23/2005	323
TH31-21	21	501357	1274269	10/20/2005	270
TH31-36	36	501357	1274269	3/24/2005	1205
TH31-36	36	501357	1274269	10/21/2005	1140
TH51-12	12	501288	1273851	1/3/2006	182
TH51-20	20	501288	1273851	4/25/2005	807
TH51-20	20	501288	1273851	1/3/2006	992
TH51-55	55	501288	1273851	4/26/2005	1212
TH71-12	12	500938	1273415	March, 2005	3
TH71-12	12	500938	1273415	10/13/2005	7
TH71-20	20	500938	1273415	3/3/2005	121
TH71-44	44	500938	1273415	3/2/2005	373
TH71-44	44	500938	1273415	10/13/2005	408